Edgeless planar semiconductor sensors for a Medipix3-based radiography detector

Bosma, M.J.; Heijne, E.; Kalliopuska, J.; Visser, J.; Koffeman, E.N.

DOI
10.1088/1748-0221/6/11/C11019

Publication date
2011

Document Version
Final published version

Published in
Journal of Instrumentation

JINST

PUBLISHED BY IOP PUBLISHING FOR SISSA

RECEIVED: *November 15, 2011*
ACCEPTED: *November 15, 2011*
PUBLISHED: *November 24, 2011*

13th INTERNATIONAL WORKSHOP ON RADIATION IMAGING DETECTORS,
3–7 JULY 2011,
ETH ZURICH, SWITZERLAND

Edgeless planar semiconductor sensors for a Medipix3-based radiography detector

M.J. Bosma,[a,1] **E. Heijne,**[a,b,c] **J. Kalliopuska,**[d] **J. Visser**[a] **and E.N. Koffeman**[a]

[a] *Nikhef, National Institute for Subatomic Physics,*
Science Park 105, 1098 XG Amsterdam, The Netherlands
[b] *CERN, European Organization for Nuclear Research,*
CERN CH-1211, Geneva 23, Switzerland
[c] *IEAP/CTU, Institute of Experimental and Applied Physics/Czech Technical University in Prague,*
Horská 3a/22, 128 00 Prague 2, Czech Republic
[d] *VTT Micro and Nanoelectronics,*
Tietotie 3, Espoo, FI-02044 VTT, Finland

E-mail: mbosma@nikhef.nl

ABSTRACT: We study the influence of active edges on the response of edge pixels by comparing simulations of the electrostatic-potential distribution to position-defined measurements on the energy deposition. A laser setup was used to measure the edge-pixel response function and shows the sensitive edge is only about 2 μm from the physical edge. 3D reconstruction of tracks from high-energy pions and muons, produced at the SPS H6 test beam facility at CERN, enabled to relate the energy deposition at edge pixels to the particle's interaction depth. A clear correlation is observed between the simulated electric-field distortion and the reconstructed interaction-depth dependent effective size.

KEYWORDS: Hybrid detectors; Detector modelling and simulations II (electric fields, charge transport, multiplication and induction, pulse formation, electron emission, etc); Particle tracking detectors (Solid-state detectors); X-ray radiography and digital radiography (DR)

[1] Corresponding author.

doi:10.1088/1748-0221/6/11/C11019

Contents

2011 JINST 6 C11019

Introduction. Due to its advanced pixel circuitry, the Medipix3 chip [1] will be an interesting read-out alternative to today's TFT and CCD-based digital radiography detectors. Bump-bonded to a mono-crystalline semiconductor sensor, it can provide electronic-noise free and fine-grained colour X-ray images of high contrast. Nevertheless, the limited active area of both the chip and high-Z single-crystal sensor wafers currently prevents replacement of large-area X-ray imaging systems. A seamless tessellation of multiple detector modules with edgeless sensors could solve this. The use of active edges seems to be an appropriate way to safely reduce the distance between the pixel matrix and the physical edge of the sensor to a few tens of microns only [2, 3]. Doped edges, however, alter the electric field locally and therefore affect the charge transport in edge pixels. This is studied by comparing simulations of the potential distribution at the edge to measurements on the effective volume of edge pixels.

1 The sensor

Prototype sensors were fabricated on 150 μm thick float-zone ν-type silicon [4]. Heavily doped n-type circular implants of 28 μm diameter at 55 μm pitch form the pixel matrix. Between the pixels a p^{++} implant, a so called p-stop, isolates the pixels from each other. A very heavily doped boron layer at the back side forms the junction and also functions as the back electrode. In order to minimise the thickness of the entrance window, it was decided to deposit no metal there. A shallow boron implant was realised at the edge by ion implantation at a slight angle to the side face. In order to be able to access the edges, the wafer was mounted on a support wafer and trenches between the sensors were etched using inductively coupled plasma etching [5] (see figure 1(a)). The distance between the edge-side of the outer pixel implants and the physical edge of the sensor is 50 μm.

Two of these sensors were flip-chipped to Timepix read-out chips and mounted side-by-side on a quad carrier board (see figure 1(b)). The module is read out through the Relaxd interface board [6, 7].

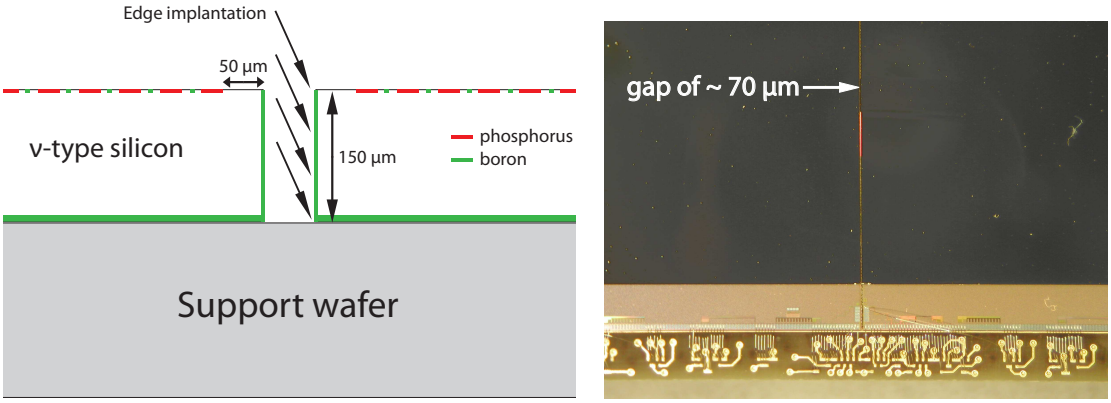

(a) (b)

Figure 1. *The detector module.* (a) Schematic view of the edge implantation step. A support wafer was needed in order to be able to access the side-walls. (b) Two edgeless-Timepix assemblies mounted side-by-side on the quad carrier board. Due to the larger size of the Timepix chip, it extends from under the sensor. This causes a small gap of approximately 70 μm between the adjacent edges of the sensors.

2 Simulations

Both the intensity- and energy-response of the detector to homogeneous irradiation with a micro-focus X-ray tube show anomalies at the edge pixels. The outermost pixels record less and lower pulses, whereas the second outer ones are considerably more sensitive. Simulations of the electrostatic-potential distribution at the edge indicate the reason for this (see figure 2). The edge implant distorts the electric field close to the edge, as a result of which the effective volume of the two outer-column pixels differs from that of more central pixels. To validate these simulations, the edge-pixel response was studied using a near-infrared laser as well as a high-energy particle beam.

3 Measurements

Position-defined measurements on the energy deposition were made with two main objectives in mind: (i) to determine the edge-pixel response function, from which the edge of the sensitive volume could be derived and (ii) to map the electric-field distribution at the edge by relating the recorded amount of energy deposition to the interaction depth. All measurements were made at -40 V sensor bias and the energy response was corrected by subtracting a fixed offset in order to exclude the non-linear part of the Timepix energy calibration curve [8].

3.1 Laser data

Monochromatic photon pulses of 683 nm and 976 nm centre wavelength, produced by two lasers, were used to determine the edge-pixel response function. By using photons of two different wavelengths, the charge collection of the pixel was studied in two different interaction volumes, the depth of which is determined by the 1/e photon absorption depth (table 1). The back side of the detector was illuminated at normal incidence and pixels were scanned with steps of 1 μm using a

2011 JINST 6 C11019

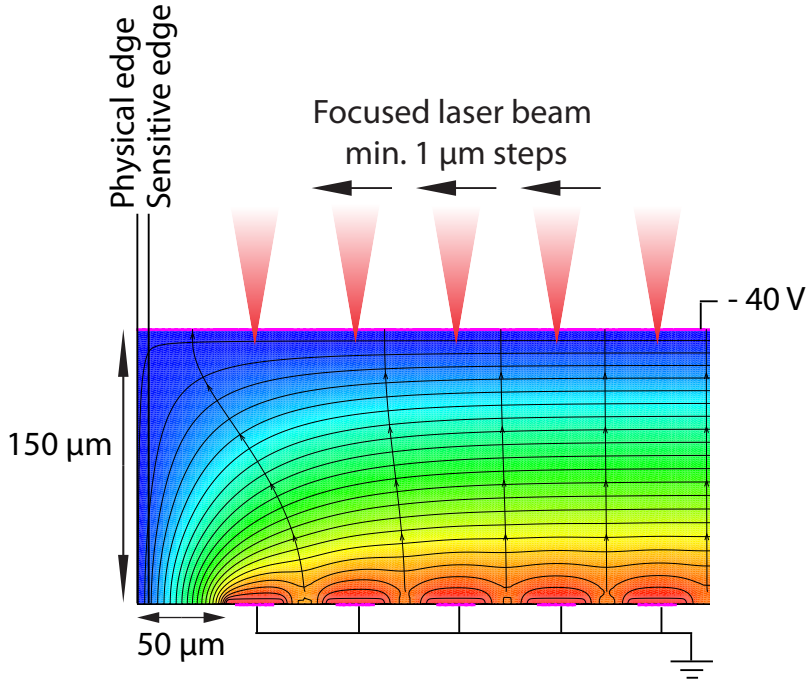

Figure 2. *Electrostatic-potential distibution.* Simulation of the potential distribution at the edge. The active edge locally distorts the electric field. A dedicated laser setup is used to study the pixel response with sub-pixel resolution, e.g. to determine the edge of the sensor's sensitive volume.

Table 1. *Photon absorption depth.* The absorption depth is determined by the photon energy and the band-gap of the material, i.e. 1.12 eV for silicon. Listed are the absorption coefficients α for the centre wavelength of the lasers.

λ [nm]	E [eV]	α [cm^{-1}]	1/e abs. depth [μm]
683	1.88	1.9×10^3	5.3
976	1.27	7.1×10^1	1.4×10^2

motorised X-Y table with closed-loop control (see figure 2). The lasers were controlled by a pulse generator and their light output was focused on the detector using a lens.

The diameter of the detected part of the laser induced charge cloud — which is mainly determined by the focal spot size and the charge-carrier diffusion — was determined to be 40 μm by recording the fractional charge deposition in several pixels in the centre of the matrix while shifting the detector with 2 μm steps in one dimension. The edge of the sensitive volume was determined in a similar way. The laser was scanned from the centre of the fifth pixel towards the edge with decreasing step size and the mean energy deposition was assigned to the laser's spot centre position with respect to the physical edge (see figure 3). For both wavelengths, the sensor stopped responding at approximately 20 μm beyond the physical edge. As this distance corresponds to the observed charge-cloud radius, it indicates a very small insensitive edge region. This is important, since the sensor's suitability for tiling is determined by the ratio between the active area and the total area of the sensor. Normalising the integrated response function of the four-outer-column

2011 JINST 6 C11019

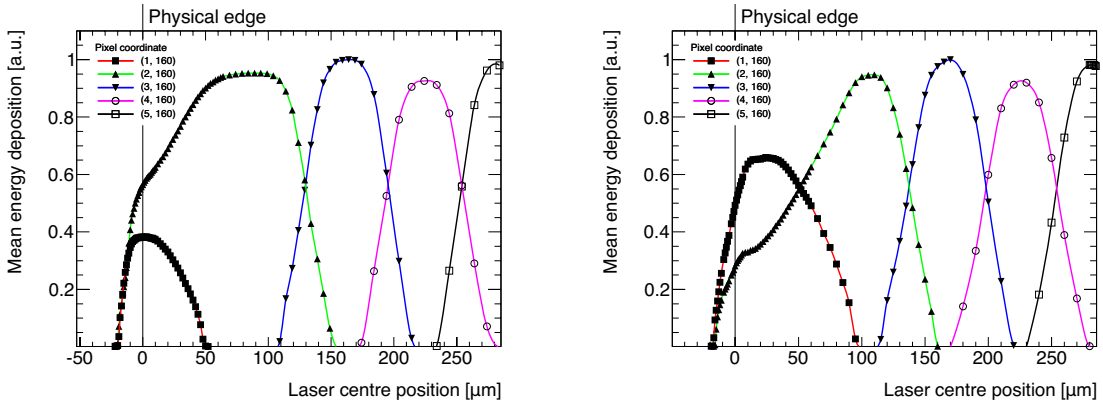

(a) 683 nm (b) 976 nm

Figure 3. *Edge-pixel response function.* The mean energy deposition recorded by single edge pixels as a function of the laser spot centre position with respect to the physical edge, for both (a) 683 nm photons and (b) 976 nm photons. Back side illumination.

pixels to four times the integrated response function of a centre pixel, results in an effective volume of 4.62 pixels, which confirms the sensitive edge is very close to the physical edge:

$$256.5\ \mu\text{m (physical width)} - 4.62 \times 55\ \mu\text{m (effective width)} \approx 2\mu\text{m}$$

In addition, figure 3 shows that pixels of the first column are smaller in effective size, whereas the second-column ones are larger. In agreement with simulations on the electric field the effect is less pronounced in the case of illumination with 976 nm photons. These photons have a larger absorption depth and therefore more photons are near the pixel plane. As a result, there is less diffusion and less influence by the electric-field distortion.

3.2 Test-beam data

The depth dependence was studied further at the SPS H6 test beam facility at CERN using tracks from 120 GeV/c muons and pions. To be able to relate the interaction depth to the amount of energy deposition in edge pixels, finite-length tracks that cross the adjacent edges in the middle of the module were needed. The module was positioned longitudinally to the beam, which allowed the particles to traverse both sensors (only 150 μm thick) practically parallel to chips' planes and thus created long ionisation tracks. Accurate 2D track reconstruction was ensured by a small elevation angle, which caused charge sharing. A shallow inclination angle provided long but finite-length tracks, the entry and exit point of which was used for 3D reconstruction.

Candidate tracks were selected by finding linear patterns using the Hough transform [9]. After this selection, a simple bubble sort algorithm was used to exclude outliers that were in line with the tracks. For each found candidate track, its length was used as a selection cut for linear fitting using a weighted least-squares method (i.e. the position of each hit was weighted by the amount of energy deposition). Fitting tracks that traverse both sensors with a single line, ignores the fact there is a small gap and slight misalignment between the detectors. To be able to do so, their relative position was determined by separately fitting the track segment in each of the sensors. From this, the gap and the rotational difference between the two assemblies could be derived and corrected.

2011 JINST 6 C11019

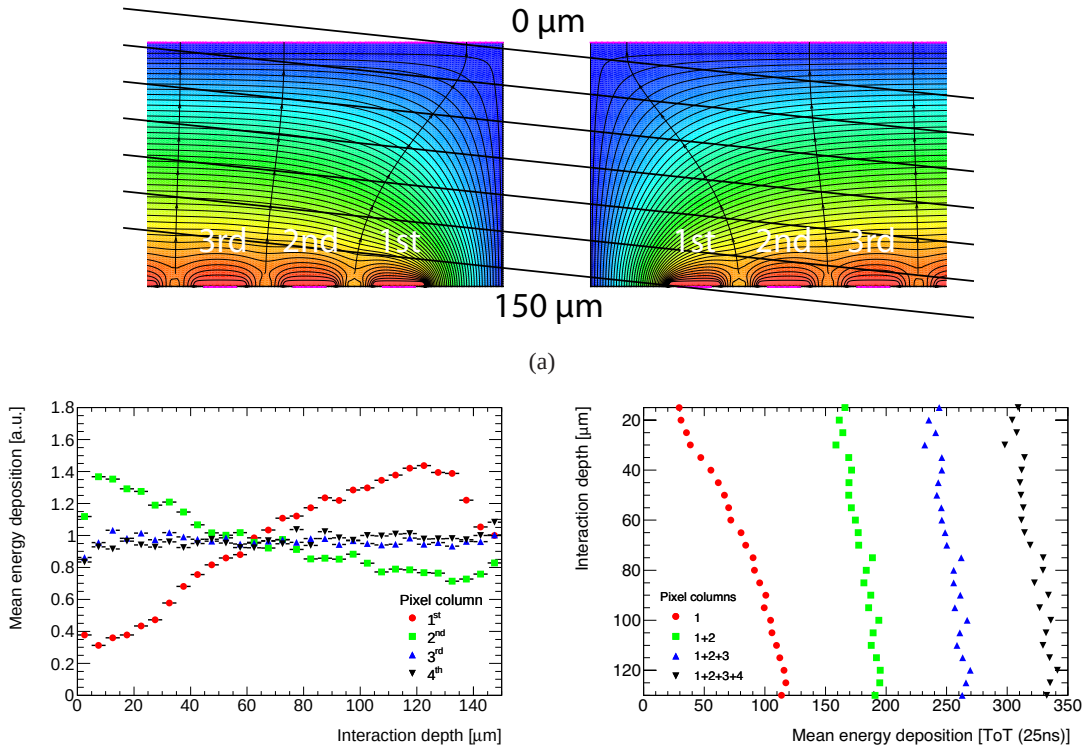

Figure 4. *Interaction-depth dependence.* (a) 3D reconstruction of shallow-angled tracks that traverse the adjacent-edge region enables to determine the interaction depth in edge pixels. (b) The mean energy deposition in pixels of the four outer columns as a function of the interaction depth. (c) The cumulative energy response as a function of the interaction depth. The plot is rotated by 90 degrees to show the correlation between the simulated pixel-separating field lines and the data.

Subsequently — knowing the gap between the sensors and the elevation and inclination angle of each individual track — the track's entry and exit point were used to reconstruct the mean interaction depth in edge pixels (see figure 4(a)). This depth is related to the amount of energy deposition. Since the energy deposition is proportional to the particle's path length through the pixel, it reflects the pixel's effective size at a certain depth. Figure 4(b) shows the mean energy deposition in pixels of the four outer columns as a function of the interaction depth and shows a correlation with the simulated effective volume. To visualise this, figure 4(c) shows the cumulative energy response of the four outer pixels — which is proportional to the total path length — as a function of the interaction depth. The similarity with the field lines that separate the pixels from each other is clear, which demonstrates a good understanding of the anomalous response of edge pixels and may allow to correct for this.

4 Summary and conclusion

The use of active edges is an appropriate way to reduce the insensitive edge of the sensor to a few tens of microns only. The electric field close to the edge, however, is distorted and affects

2011 JINST 6 C11019

the edge-pixel's response. Simulations on the electrostatic field distribution show the effective volume is depth dependent and therefore differs from that of more central pixels. The edge doping bounds the depletion region and therefore a small but non-negligible part of the sensor volume is lost inevitably. Nevertheless, laser measurements showed that the edge of the sensor's sensitive volume is only about 2 μm from the physical edge. Measurements on the depth dependence of the edge-pixel's effective size show excellent agreement with the simulations. Plots on the cumulative response even reveal resemblance to electric-field lines. This demonstrates the simulations are reasonably realistic and may be used to correct for the anomalous edge-pixel response.

Acknowledgments

We gratefully acknowledge the help of Richard Plackett and Martin van Beuzekom during the beam tests at CERN and we are thankful for the continuous support of Joop Rövekamp and Bas van der Heijden. The sensors have been manufactured and processed by VTT Micro and Nanoelectronics, Espoo, Finland. The work has been supported by Dutch Ministry of Economic Affairs.

References

[1] R. Ballabriga et al., *Medipix3: a 64k pixel detector readout chip working in single photon counting mode with improved spectrometric performance*, *Nucl. Instrum. Meth.* **A 633** (2011) S15.

[2] C.J. Kenney et al., *Active-edge planar radiation sensors*, *Nucl. Instrum. Meth.* **A 565** (2006) 272.

[3] M.J. Bosma et al., *Edgeless silicon sensors for medipix-based large-area x-ray imaging detectors*, 2011 *JINST* **6** C01035.

[4] J. Kalliopuska et al., *Characterization of edgeless pixel detectors coupled to Medipix2 readout chip*, *Nucl. Instrum. Meth.* **A 648** (2011) S32.

[5] Y.Q. Fu et al., *Deep reactive ion etching as a tool for nanostructure fabrication*, *J. Vac. Sci. Technol.* **B 27** (2009) 1520.

[6] Z. Vykydal et al., *The RELAXd project: development of four-side tilable photon-counting imagers*, *Nucl. Instrum Meth.* **A 591** (2008) 241.

[7] J. Visser et al., *A gigabit per second read-out system for Medipix quads*, *Nucl. Instrum Meth.* **A 633** (2010) S22.

[8] J. Jakubek et al., *Pixel detectors for imaging with heavy charged particles*, *Nucl. Instrum Meth.* **A 591** (2010) 165.

[9] R.O. Duda and P.E. Hart, *Use of the Hough transformation to detect lines and curves in pictures*, *Commun. ACM* **15** (1972) 11.

2011 JINST 6 C11019